Elaboration and rheological characterization of nanocomposite hydrogels containing C 60 fullerene nanoplatelets

Théo Merland, Mathieu Berteau, Marc Schmutz, Stéphanie Legoupy, Taco Nicolai, Lazhar Benyahia, Christophe Chassenieux

ARTICLE

Elaboration and rheological characterization of nanocomposite hydrogels containing C_{60} fullerene nanoplatelets

Received 00th January 20xx,
Accepted 00th January 20xx

DOI: 10.1039/x0xx00000x

Théo Merland,*[a,b] Mathieu Berteau, [a] Marc Schmutz, [c] Stéphanie Legoupy, [d] Taco Nicolai, [a] Lazhar Benyahia, [a] and Christophe Chassenieux[a]

Nanocomposite hydrogels were elaborated that consisted of a physical network formed by an amphiphilic polymer in which C_{60} fullerene nanoplatelets were embedded. Characterization showed that the nanoplatelets within the polymer network were aggregated. The presence of these nanoplatelets led to an increase of the shear modulus of the hydrogels, that cannot be explained by a filler effect alone. The nanocomposite gels displayed similar rheological behavior, both in linear and non-linear domains, as neat hydrogels at higher polymer concentrations. We suggest that the particles reinforced the gels by forming additional connections between the polymer chains.

Introduction

Polymer hydrogels are an attractive class of materials because of their ability to resist flow under gravity even though they mainly contain water, which is advantageous for ecological, health and economic reasons. They consist of a polymer matrix swollen by water. Two types of hydrogels can be distinguished. Chemical gels, where the polymer chains are covalently crosslinked, display stronger mechanical properties but cannot self-heal after breaking.[1] Physical gels rely on temporary junctions that allow the gels to recover after rupture, but have weaker mechanical properties than chemical gels in general.[2] However, hydrogels are brittle and poorly deformable because of their low ability to dissipate stress and possibly due to structural defects leading to heterogeneities of the networks.[3-5]

Therefore, several strategies are adopted to reinforce hydrogels, such as enhancing the homogeneity of the networks by using well-defined chemical structures,[6-8] building a second polymer network that can act as a sacrificial network,[7, 9, 10], adding electrostatic interactions[10-13] or incorporating solid particles that interact specifically with the polymer matrix, yielding nanocomposite hydrogels.[14-16] These particles act as dissipaters under stress. Nanocomposite hydrogels display higher elastic moduli than neat hydrogels, and can bear higher strains and stress before breaking.[14] Their high deformability comes from the alignment of the particles in the perpendicular direction to stress, allowing the polymer chains linked to them to stretch.[17-19] Since bonds are established between particles and polymer chains, there is no need to crosslink the polymer chains directly.[20] Most nanocomposite hydrogels rely on hydrogen bonding by using clay or silica particles, but other weak interactions can also be exploited, such as hydrophobic interactions or π-π stacking, e.g. by using nanocarbons as reinforcing particles. In most cases, carbon nanotubes[21, 22] and graphene oxide[23, 24] are used thanks to their thermal or electrical properties. However, their use in aqueous media is hindered by the difficulty to exfoliate them.[25]

It could thus be of interest to incorporate functional particles in polymer hydrogels to bring additional properties on top of mechanical reinforcement. In particular, for the design of organic photovoltaic devices, fullerene is often used as electron acceptor.[25] Fullerene is also used as an efficient antibacterial material in aqueous medium.[26, 27] To design gels that encapsulate fullerene will therefore have good potential for application. However, since fullerene is poorly soluble in water, it is often used in organic solvents which are toxic and pollutant.[25] For this reason, only few examples of fullerene-containing hydrogels are reported in literature.[28, 29] Wakai et al. reported hydrogels obtained by self-assembly in water of fullerene derivatives bearing poly(ethylene glycol) (PEG) chains.[30] Another study described physical hydrogels resulting from complexation of modified fullerene with a peptide.[29] In both cases, a major drawback of these gels is that they required chemical modification of fullerene, that is often extensive and can deteriorate the physical properties of fullerene. Only one study reported the incorporation of pure C_{60} in hydrogels, and did not give insight into the mechanical nor opto-electrical properties of the gels.[31] Therefore, there is an open field for the design of hydrogels containing pure C_{60}. In particular, dynamic physical gels would be of

[a] Institut des Molécules et Matériaux du Mans, UMR CNRS 6283, Le Mans Université, Avenue Olivier Messiaen, 72085 Le Mans Cedex 9, France.
[b] Soft Matter Sciences and Engineering, ESPCI Paris, PSL University, Sorbonne University, CNRS, F-75005 Paris, France.
[c] Université de Strasbourg, CNRS, Institut Charles Sadron, UPR 22, 23 Rue du Loess, 67034 Strasbourg Cedex, France.
[d] Université d'Angers, MOLTECH-ANJOU, UMR CNRS 6200, F-49000 Angers, France.
Electronic Supplementary Information (ESI) available: [details of any supplementary information available should be included here]. See DOI: 10.1039/x0xx00000x

great interest for the formulation of inks[32, 33] that would contain stable fullerene particles at rest and flow under stress.

We recently reported the formation of C_{60} nanoplatelets in water mediated by an amphiphilic polymer.[34] This polymer is able to yield physical gels behaving as yield-stress fluids for concentrations higher than 4 wt%.[35] Therefore, we propose the incorporation of fullerene nanoplatelets within these hydrogels since we already know that they interact strongly with the polymer. Here we describe the synthesis of the hydrogels, the characterization of the dispersion state of the fullerene nanoplatelets in them and their dynamic mechanical properties.

Experimental section

Materials. Carbon disulfide (Sigma-Aldrich, >99.7%), toluene (Thermo Fischer, analytical reagent grade) and ultrapure water (Millipore) were used as received. C_{60} fullerene was purchased from MST-Nano Ltd. (Saint-Petersburg, Russia) with a purity higher than 99.9%. It was dissolved in excess in carbon disulfide over 24h under magnetic stirring in aluminium-foiled vials. The concentration of these saturated solutions was 7.6 g/L as determined by UV-visible spectroscopy. They were stored in the dark and filtered through 0.2µm pore size filters prior to use.

Polymer synthesis. Amphiphilic copolymer 75C12 was synthesized according to procedure described by Limouzin-Morel et al.[36] A copolymer with 75 mol% grafted units was thus obtained with $M_n=4.10^4$ g/mol and Đ=1.5 as determined by size exclusion chromatography. Solutions of 75C12 in ultrapure water were obtained by mixing both components and heating the mixtures at 80°C in a thermostated bath overnight.

Preparation of nanocomposite hydrogels. The preparation of suspensions of fullerene nanoplatelets has been reported elsewhere.[34] Briefly, 1.6 mL of fullerene saturated solution in carbon disulfide were mixed with 2.4 mL of 75C12 solution in ultrapure water with C_{pol}=10 g/L. The system was emulsified using an ultrasonic horntip with a frequency of 20 kHz and an amplitude of 36%. The ultrasound treatment was pursued continuously, causing heating of the emulsion and therefore evaporation of carbon disulfide. Sonication proceeded until full removal of CS2, which took ca. 8 minutes. During this process the sample lost its milky aspect and turned into a brownish turbid solution. The dispersion had a fullerene concentration of 4 g/L as determined by UV-visible spectroscopy. The operation was repeated in parallel several tens of times. Then all the dispersions were gathered into a round-bottom flask and freeze-dried. The obtained composite powder, as well as pure polymer and fullerene, were analyzed by TGA between 20 and 1100°C to quantify the content of polymer and fullerene, see next section. The composite powder consisting of fullerene nanoplatelets embedded in the amphiphilic polymer was subsequently dispersed in ultrapure water and heated at 80°C overnight to obtain nanocomposite hydrogels. In some cases, composite powders were mixed with neat polymer (also in the form of powder) in order to vary polymer and fullerene concentrations. This procedure had no influence on the rheological properties of the gels (see Figure S1), which indicated that the amount of remaining solvent should be below the ppm scale. For light scattering and UV-visible spectroscopy, samples were diluted down to ca. 5 mg/L fullerene by diluting a small amount of gel in ultrapure water followed by a thermal treatment at 80°C for at least two hours.

Thermogravimetric analysis. The composite powders consisting in fullerene nanoplatelets embedded in amphiphilic polymer were analyzed with a TGA 2 (Mettler Toledo, USA). 10 mg of powder were heated from 20 to 1100°C with a 10°C/min temperature ramp under nitrogen flow at 80 mL/min. Four weight losses were noticed at ca. 100°C (water loss), 250 and 400°C (polymer), and 800°C (fullerene, in good agreement with literature)[37], see Figure S2. The amount of fullerene in composite powders was determined as the remaining weight at 600°C, where a plateau is observed between polymer and fullerene degradation.

UV-visible spectroscopy. Fullerene concentrations in suspensions and hydrogels were determined by diluting them down to ca. 5 mg/L and measuring the UV-vis absorbance in water at the maximum around 340 nm. The absorbance was converted into fullerene concentration with an absorption coefficient equal to 105 $L.g^{-1}.cm^{-1}$ (as previously described).[34] To verify that the procedure previously used for fullerene dispersions was still reliable for nanocomposite hydrogels, the fullerene was extracted from them following the procedure described by Deguchi et al.[38] 1 mL of hydrogel dilution was mixed with 1 mL 1 wt% NaCl aqueous solution and 2 mL toluene. Then the mixture was emulsified at 3000 rpm using a Vortex shaker and the organic phase was collected after phase separation. Absorbance was measured at the maximum at 336 nm and concentration was computed using Beer-Lambert law with an absorption coefficient equal to 87 $L.g^{-1}.cm^{-1}$ (as determined by calibration curve). Both values of fullerene concentration obtained from measurements in water and toluene were in good agreement as shown in a previous work.[34]

Light Scattering. Measurements were done at 20°C on a CGS-3 (ALV GmbH, Germany) compact system with an LSE-5004 correlator and a laser having a wavelength of 632.8 nm. The scattering intensity and auto-correlation function were measured as a function of the scattering angle (θ) from 12° to 150°. The apparent molar mass, gyration and hydrodynamic radii were obtained from these data as detailed in Supporting Information.

Cryo-Transmission Electron Microscopy (cryo-TEM). A lacey carbon film (Ted Pella) supported on a copper grid was hydrophilized with a glow discharge (Elmo-Cordouan Technologie). 5 µL of the solution were then directly deposited on the film. The solution was blotted to form a thin film with a home-made freezing machine (T=22°C and humidity 80 % RH) and the grid was rapidly immersed in a liquid ethane bath maintained at the liquid nitrogen ebullition point, in order to form an amorphous ice layer containing well-preserved structures. The grid was then transferred under liquid nitrogen on a Gatan 626 cryo-holder and transferred into the TEM (Tecnai G2 sphera FEI). The grids were observed under low dose conditions at 200 kV and images taken with an Eagle 2K ssCCD camera (FEI).

Rheology. Measurements were carried out at 20°C on a Discovery HR-3 rheometer (TA Instruments) using a cone-plate geometry with 20 mm diameter, 28 µm truncature and 1°0'2'' angle. For all samples, the samples were studied at steady state and the linear domain was determined at an angular frequency of 10 rad/s prior to frequency-dependent measurements at 1 % strain, which was in the linear domain for all samples. Low-viscosity paraffin oil was deposited around the sample to prevent any water evaporation.

Results

Elaboration of hydrogels. As explained in the experimental section, composite powders consisting in the amphiphilic polymer 75C12 and C_{60} fullerene were prepared by freeze-drying a large quantity of aqueous colloidal suspensions. The composition of the composite powders was obtained by TGA, see experimental section and Figure S1. The nanocomposite hydrogels were obtained through re-dispersion of the composite powders in water. In this way, several series of hydrogels were prepared with either constant fullerene or polymer concentration, respectively noted C_{full} and C_{pol}. The polymer concentration was deduced from the polymer content in the composite powder. C_{full} values were computed from UV-visible absorption spectra measured in water, see experimental section. In this way, hydrogels with C_{pol} ranging from 33 to 58 g/L keeping constant C_{full} to 10 g/L were obtained, as well as samples with constant C_{pol}=40-50-65-85-100 g/L and various values of C_{full} comprised between 0 and up to 50 g/L. The latter concentration is, to our knowledge, the highest concentration ever reported for fullerene in aqueous medium up to date, the previous one being 8 g/L.[34]

Dispersion state of nanoplatelets. The dispersion state of particles within the hydrogels was assessed by cryo-TEM and static light scattering as shown in Figures 1/S3 and S4, respectively. Both techniques show that the nanoplatelets are aggregated when embedded in the hydrogels, whereas they were individually dispersed in the aqueous suspension. The cryo-TEM images show that the nanoplatelets remain intact, but several are stacked on top of each other. Static light scattering results indicate a general increase of the scattering intensity after the drying/re-dispersion treatment. At low q values, the plateau value which is equal to the weight average molar mass is increased by two orders of magnitude by comparison with the original dispersion. The angular dependency of the scattered intensity is also stronger after freeze-drying, indicating an increase of the gyration radius. However, all the samples displayed reproducible scattering profiles, which means that no matter the concentration at which they were prepared, the aggregation state of C_{60} particles was the same. From this we can conclude that the nanoplatelets aggregate during freeze-drying and the re-dispersion at 80°C fails to break these aggregates. One attempt to promote exfoliation consisted of magnetic stirring or sonication during this step. However, due to the high viscosity of the dispersions, the nanoplatelets remained aggregated.

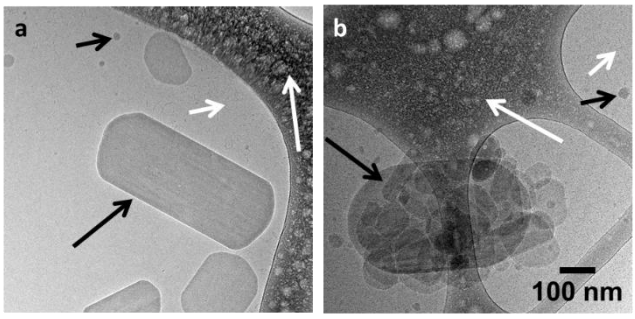

Figure 1. Representative cryo-TEM pictures of C_{60} nanoplatelets dispersion in water before (a) and after redispersion following their freeze drying (b). Short white arrows show micelles (spherical + worm-like) formed by self-assembly of 75C12; long white arrows show the carbon-lacey supporting membrane; long black arrows show fullerene nanoplatelets; short black arrows show isotropic fullerene nanoparticles. Some higher magnifications of the same pictures are shown in the Supporting Information (Figure S3).

It should be mentioned that prior to cryo-TEM and light scattering analysis, the samples have been diluted. For cryo-TEM, the samples were diluted in order to decrease their viscosity (down to C_{pol}=10 g/L and C_{full}=4 g/L). For light scattering, the samples were diluted approximately thousand-fold to avoid light absorption. Maybe the nanoplatelets were less aggregated before dilution as in general, the presence of macromolecules at high concentration helps exfoliating such 2D nanoparticles by intercalating between the particles.[39, 40] It should be mentioned that we observed the presence of a minority of isotropic nanoparticles, which are aggregates of fullerene. They remained intact after re-dispersion.

Linear rheological properties. The mechanical properties of the nanocomposite hydrogels were assessed by rheology. In Figure 2, the storage (G') and loss (G'') moduli, accounting respectively for the elastic and viscous contributions of the hydrogels, are plotted as function of the angular frequency (ω). All the hydrogels behaved as viscoelastic liquids since at low frequency, G'<G'' and exponents of 2 and 1 (expected for liquids) were observed respectively for G' and G'' as function of frequency. G' and G'' crossed at a frequency ω_c and at high frequency, G'>G''. However, no plateau value for G' is observed at high frequency, where it is expected for a viscoelastic liquid where G' should tend to a constant value equal to the shear modulus (G) describing the stiffness of the network. That is why the shear modulus of the gel has been considered as being the value for G' at $\omega=100\omega_c$. When fullerene particles are added to the hydrogel matrix with C_{pol}=50 g/L, an increase of both G' and G'' is observed. Adding particles gradually increases G up to a factor 4 for a fullerene concentration of 13 g/L. Interestingly, the crossing of G' and G'' is shifted to lower frequencies when particle concentration increases, which means that the average relaxation time is increased.

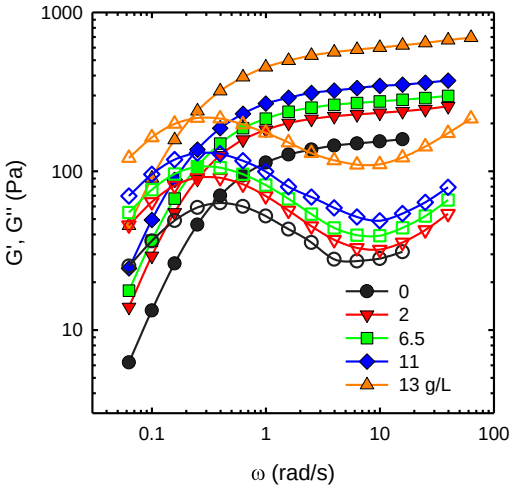

Figure 2. Evolution of storage (closed symbols) and loss (open symbols) moduli over angular frequency for various fullerene concentrations (indicated in legend) at C_{pol}=50 g/L and T=20°C in the linear response regime.

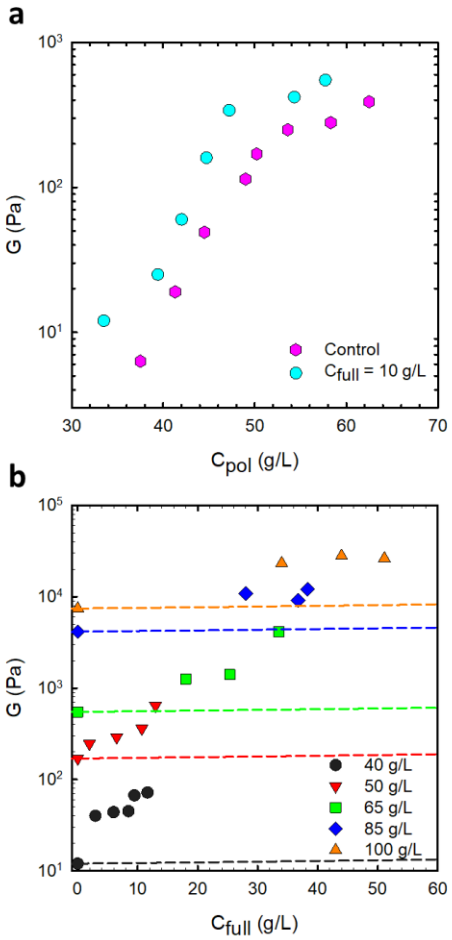

Figure 3. Evolution of the shear modulus at 20°C as a function of a) polymer concentration for hydrogels without (pink hexagons) or with 10 g/L (blue circles) particles. b) Elastic modulus vs fullerene concentration for hydrogels with various polymer concentrations indicated in legend. The dashed lines correspond to the Guth & Gold model computed from Eq.1.

Figure 3a displays the evolution of the shear modulus with C_{pol} for neat and composite hydrogels with a constant concentration of fullerene particles of 10 g/L. The polymer concentration dependence of G displays the same pattern for neat and nanocomposite hydrogels but the increase of G occurs at lower C_{pol} for the composite hydrogels which means that the percolation concentration was shifted to lower C_{pol} in presence of fullerene nanoparticles. Elastic moduli were systematically higher in presence of fullerene for a fixed C_{pol}.

Figure 3b displays the shear modulus variation upon C_{full} for constant C_{pol} values. Nanocomposite hydrogels were systematically stiffer than control samples, and increasing the particles concentration resulted in an increase of shear modulus. The effect is more important for lower C_{pol} values. For example, a hydrogel with C_{pol}=40 g/L and C_{full}=12 g/L displayed a 6-fold higher shear modulus compared to the control, while a gel with C_{pol}=100 g/L and C_{full}=50 g/L had a G value 4 times higher than the neat one. When considering the complex viscosity, defined as $\eta^* = \frac{1}{\omega}\sqrt{G'^2 + G''^2}$,

instead of shear modulus, the same conclusion can be drawn (Figure S5).

The influence of temperature on the rheological properties of the gels was also studied by carrying out frequency sweeps at temperatures ranging from 20 to 60°C, see Figure S6a. The gels displayed a viscoelastic liquid behavior. G' and G" were found to cross at higher frequencies when the temperature was increased implying that the terminal relaxation time decreased. A time-temperature superimposition was obtained by shifting the frequency with a coefficient a_T with respect to a reference temperature (Figure S6b). The shift factors a_T display an Arrhenius temperature dependence, see Figure S6c. The corresponding activation energy is equal to 140 kJ/mol for both composite and neat hydrogels, in agreement with previous observations for the latter.[35]

Non-linear rheological properties. The behavior of the hydrogels under strain was studied by applying increasing oscillatory stress on the hydrogels. Control and nanocomposite hydrogels were compared at *iso*-C_{pol} (Figure 4). In all cases, at low strain, a linear dependency of stress over strain is characteristic of the linear regime. In this regime, $\sigma=G.\gamma$, with σ the stress, G the shear modulus and γ the strain, for a given frequency and temperature.

All gels (control or nanocomposites) with low elastic moduli displayed shear-thickening before rupture (see Figure S7a). However, shear-thickening was more marked in the presence of particles. The yield stress and strain, noted respectively σ_y and γ_y, were taken at the point where stress reached its maximum value. Beyond this value, the stress reaches a plateau value, which can be attributed to shear-banding that is often observed in associative polymer networks.[41] Therefore, these points were not considered. Control and nanocomposite hydrogels with higher elastic moduli (typically more than 10^3 Pa) did not show shear-thickening, see Figure S7b.

The yield stress increased with increasing particles concentration (Figure S8a), to a lower extent than shear modulus, whereas the yield strain slightly decreased (Figure S8b).

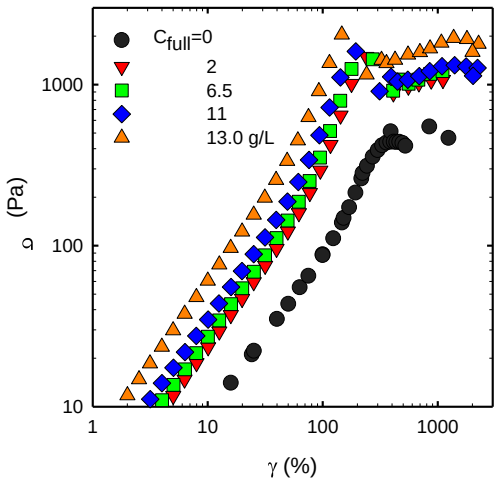

Figure 4. Stress-strain curves obtained at T=20°C, ω=10 rad/s for hydrogels with C_{pol}=50 g/L, for various fullerene concentrations as indicated in the figure.

Discussion

Influence of fullerene particles on the stiffness. The increase of the stiffness for the composite hydrogels may be due either to specific interactions between the particles and the polymer network or to a filler effect of the former. In the latter case, the Guth & Gold model accounts for the increase of the shear modulus of the matrix alone (G_0)[20, 42] according to:

$$G = G_0(1 + 2.5\Phi_p + 14.1{\Phi_p}^2) \qquad \text{Eq. 1}$$

with Φ_p being the volume fraction occupied by the particles that is:

$$\Phi_p = C_{full} \times d \qquad \text{Eq. 2}$$

with d the particles density. Considering that the particles have the same density as pristine C_{60}, we used d=1.65. The results of the model are plotted in Figure 3b and compared with the experimental data. It is clear that if particles were behaving solely as fillers, a much lower increase of G would be expected due to the low concentration of particles added to the matrix. The model considers spherical particles, but the consideration of anisotropic particles barely modifies it.[43] Therefore, the reinforcement of the hydrogels by incorporation of C_{60} nanoparticles is likely to be caused by strong interactions between them and the matrix.

Accordingly, considering $G-G_0$ rather than G can give help at better specifying the contribution of fullerene particles to the network.[16] By doing so, we consider that particles form an additional network. $G-G_0$ is plotted against particles concentration for all nanocomposite hydrogels in Figure 5. All the data collapse on a single curve and follow a power law with an exponent equal to 3.5. This value is close to what can be found in literature for colloidal gels where particles strongly bind and bear stress by bending of the particles chains.[44]

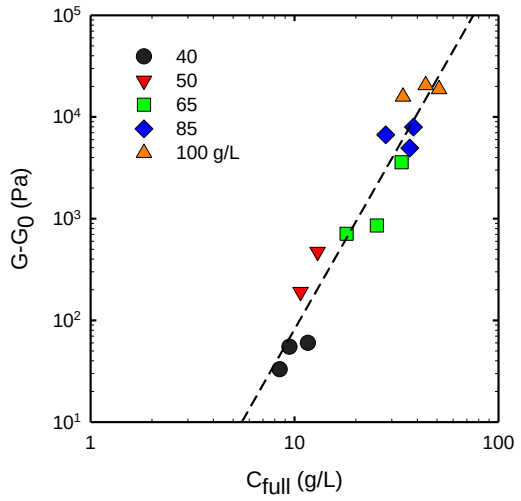

Figure 5. Reduced shear modulus as function of the particle concentration for various polymer concentrations as indicated in the figure. The dashed line represents a power law relationship with an exponent equal to 3.5.

Considering the rather low volume fraction of particles, it seems reasonable to consider that part of the polymer may act as a sticker between particles to form the additional network. However, such a network should be quite loose and display a lower exponent, close to 2.[45] In addition, the anisotropy of the particles should also decrease the value of the exponent as demonstrated by Kao et al.[46] The rather high value of the exponent could be explained by the heterogeneity of the network as was recently discussed by Zhang et al.[47] as a heterogeneous network has a higher percolation concentration and a larger exponent than a homogeneous one. Another possibility is that particles act as connections between polymer chains that increase the number of active elastic chains in the network. In favor of this scenario, we note the absence of a plateau value of G' at low frequencies (see Figure 2) suggesting that there is no additional network forming additionally to the polymer one.

Influence of fullerene particles on the dynamics. The increase of the average relaxation time τ in the presence of particles (Figure 2) indicates that the relaxation mechanism of the polymer is modified when C_{60} is introduced within the gel.

It was possible to build a master curve for samples containing fullerene at various concentrations for C_{pol}=50 g/L (Figure 6a). For a Maxwell fluid, the frequency dependence of G' and G'' is given by:

$$G' = G\frac{\omega^2\tau^2}{1+\omega^2\tau^2} \qquad \text{Eq. 3}$$

$$G'' = G\frac{\omega\tau}{1+\omega^2\tau^2} \qquad \text{Eq. 4}$$

with G the shear modulus, ω the angular frequency and τ the average relaxation time. Maxwell's model fails at describing the behavior of both neat and composite hydrogels, because they display a broad distribution of relaxation times. However, addition of fullerene does not broaden further this distribution. Moreover, since for whatever C_{full}, a master curve can be obtained, the relaxation of the composites hydrogels proceeds in the same way as neat ones though absolute values of relaxation time and shear modulus differ.

Also, when tan δ is plotted vs G, one can see that all data collapse on a single curve (Figure 6b), showing once again that incorporation of fullerene does not influence the shape of the distribution of relaxation times.

For low G values, tan δ values are quite high because the networks are weak, then increasing G results in a decrease of tan δ. The increase of the latter at higher G can be ascribed to the Rouse relaxation observed at high frequencies.

High deformation. The rheological properties in the high strain regime give information on the homogeneity of the network. The stress (σ_r) and strain (γ_r) at rupture, when plotted vs the shear modulus in the linear regime, followed power laws with exponents 1/2 and -1/3, respectively (see Figure 7). This means that $\gamma_r \propto {\sigma_r}^{-3/2}$ (see Figure S8c).

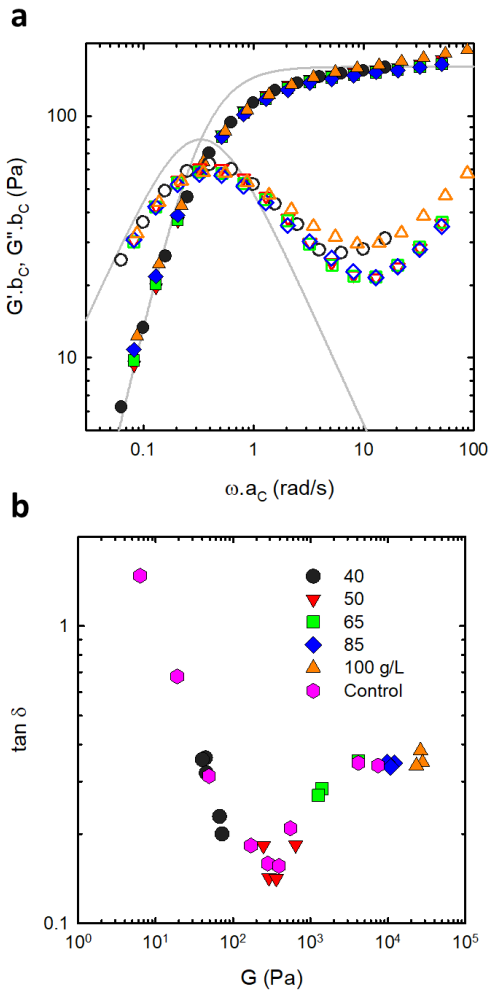

Figure 6. a) Master curve obtained by shifting data of Figure 2 with factors noted a_C (X axis) and b_C (Y axis). The reference was the sample with C_{full}=0 g/L. The gray solid lines display Maxwell model using Eq. 3&4 with G=160 Pa and τ=3s. b) Tan δ

measured at 10 rad/s as function of the shear modulus for gels with same polymer concentrations as in b), with γ=1% and T=20°C. Dashed line is a guide to the eye.

According to the Griffith model,[48] where such a scaling is predicted, the stress at rupture should scale with $(G/a)^{1/2}$, where a is the size of the defect from which the fracture originates. Since for control and nanocomposites the scaling exponent is the same, we may conclude that the homogeneity of the network is the same in both cases.

Conclusions

Nanocomposite hydrogels were obtained by co-assembling amphiphilic copolymer with C_{60} fullerene nanoplatelets. The polymer was able to self-assemble to form physical hydrogels. The addition of fullerene to the polymer network resulted in a significant increase of the shear modulus, showing strong interactions between the particles and the polymer matrix.

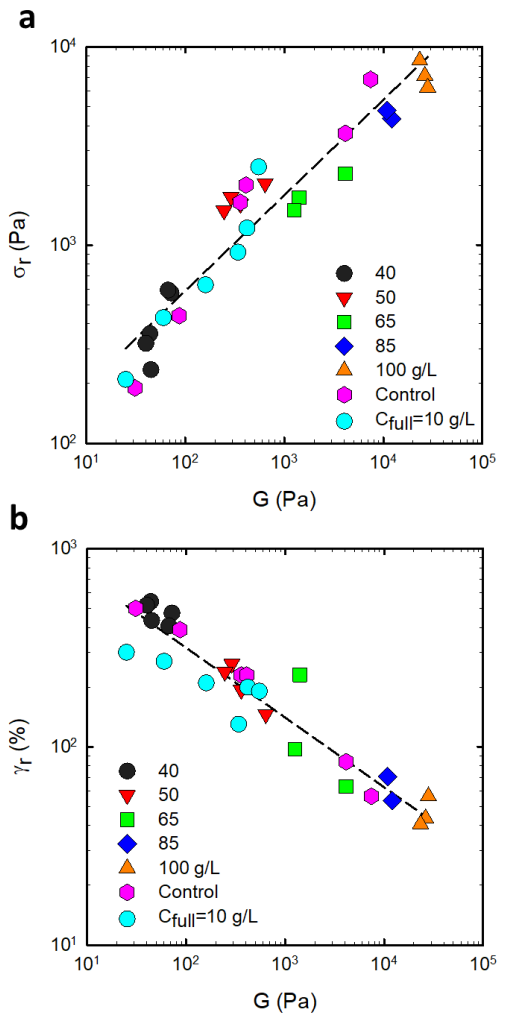

Figure 7. a) Stress at rupture expressed as function of the shear modulus. Dashed line is a power law with a slope of 1/2. b) Strain at rupture expressed as function of the shear modulus. Dashed line is a power law with an exponent equal to -1/3.

Nanocomposite hydrogels displayed similar dynamics and deformation properties as the neat polymer network. These new materials behave as yield-stress fluids, which is interesting as they can stabilize fullerene particles for months under gravity and are able to flow under moderate stress, which paves the way for the design of inks for the conception of photovoltaic devices.

Author Contributions

Théo Merland: Investigation, Writing – original draft. Mathieu Berteau : Investigation. Marc Schmutz: Investigation. Stéphanie Legoupy: Supervision. Taco Nicolai: Writing – review & editing. Lazhar Benyahia: Methodology, Writing – review & editing. Christophe Chassenieux: Conceptualization, Supervision, Writing – original draft.

Conflicts of interest

There are no conflicts to declare.

Acknowledgements

The authors acknowledge the support of Le Mans Université in the frame of the regional SPEED (Smart sustainable PolymErs and procEss Development) program. The authors thank Artem Kovalenko, Dominique Hourdet and Guylaine Ducouret for helpful discussions.

References

1. Kadam V, Nicolai T, Nicol E, Benyahia L. Structure and Rheology of Self-Assembled Telechelic Associative Polymers in Aqueous Solution before and after Photo-Cross-Linking. Macromolecules. 2011;44(20):8225-32.
2. Chassenieux C, Nicolai T, Benyahia L. Rheology of associative polymer solutions. Current Opinion in Colloid & Interface Science. 2011;16(1):18-26.
3. Dušek K, Vojta V. Concentration of elastically active network chains and cyclisation in networks obtained by alternating stepwise polyaddition. British Polymer Journal. 1977;9(2):164-71.
4. Sakai T. Experimental verification of homogeneity in polymer gels. Polymer Journal. 2014;46(9):517-23.
5. Mendes E, Oeser R, Hayes C, Boué F, Bastide J. Small-Angle Neutron Scattering Study of Swollen Elongated Gels: Butterfly Patterns. Macromolecules. 1996;29(17):5574-84.
6. Okumura Y, Ito K. The Polyrotaxane Gel: A Topological Gel by Figure-of-Eight Cross-links. Advanced Materials. 2001;13(7):485-7.
7. Tanaka Y, Gong JP, Osada Y. Novel hydrogels with excellent mechanical performance. Progress in Polymer Science. 2005;30(1):1-9.
8. Sakai T, Matsunaga T, Yamamoto Y, Ito C, Yoshida R, Suzuki S, et al. Design and Fabrication of a High-Strength Hydrogel with Ideally Homogeneous Network Structure from Tetrahedron-like Macromonomers. Macromolecules. 2008;41(14):5379-84.
9. Gong JP, Katsuyama Y, Kurokawa T, Osada Y. Double-Network Hydrogels with Extremely High Mechanical Strength. Advanced Materials. 2003;15(14):1155-8.

10. Sun J-Y, Zhao X, Illeperuma WRK, Chaudhuri O, Oh KH, Mooney DJ, et al. Highly stretchable and tough hydrogels. Nature. 2012;489(7414):133-6.
11. Spruijt E, Sprakel J, Lemmers M, Stuart MAC, van der Gucht J. Relaxation Dynamics at Different Time Scales in Electrostatic Complexes: Time-Salt Superposition. Physical Review Letters. 2010;105(20):208301.
12. Gucht Jvd, Spruijt E, Lemmers M, Cohen Stuart MA. Polyelectrolyte complexes: Bulk phases and colloidal systems. Journal of Colloid and Interface Science. 2011;361(2):407-22.
13. Lin P, Ma S, Wang X, Zhou F. Molecularly Engineered Dual-Crosslinked Hydrogel with Ultrahigh Mechanical Strength, Toughness, and Good Self-Recovery. Advanced Materials. 2015;27(12):2054-9.
14. Haraguchi K, Takehisa T, Fan S. Effects of Clay Content on the Properties of Nanocomposite Hydrogels Composed of Poly(N-isopropylacrylamide) and Clay. Macromolecules. 2002;35(27):10162-71.
15. Haraguchi K, Farnworth R, Ohbayashi A, Takehisa T. Compositional Effects on Mechanical Properties of Nanocomposite Hydrogels Composed of Poly(N,N-dimethylacrylamide) and Clay. Macromolecules. 2003;36(15):5732-41.
16. Le Goff KJ, Gaillard C, Helbert W, Garnier C, Aubry T. Rheological study of reinforcement of agarose hydrogels by cellulose nanowhiskers. Carbohydrate Polymers. 2015;116:117-23.
17. Nishida T, Obayashi A, Haraguchi K, Shibayama M. Stress relaxation and hysteresis of nanocomposite gel investigated by SAXS and SANS measurement. Polymer. 2012;53(20):4533-8.
18. Rose S, Marcellan A, Narita T, Boué F, Cousin F, Hourdet D. Structure investigation of nanohybrid PDMA/silica hydrogels at rest and under uniaxial deformation. Soft Matter. 2015;11(29):5905-17.
19. Haraguchi K. Nanocomposite hydrogels. Current Opinion in Solid State and Materials Science. 2007;11(3):47-54.
20. Carlsson L, Rose S, Hourdet D, Marcellan A. Nano-hybrid self-crosslinked PDMA/silica hydrogels. Soft Matter. 2010;6(15):3619-31.
21. Servant A, Methven L, Williams RP, Kostarelos K. Electroresponsive Polymer–Carbon Nanotube Hydrogel Hybrids for Pulsatile Drug Delivery In Vivo. Advanced Healthcare Materials. 2013;2(6):806-11.
22. Mottet L, Le Cornec D, Noël J-M, Kanoufi F, Delord B, Poulin P, et al. A conductive hydrogel based on alginate and carbon nanotubes for probing microbial electroactivity. Soft Matter. 2018;14(8):1434-41.
23. Valentin TM, Landauer AK, Morales LC, DuBois EM, Shukla S, Liu M, et al. Alginate-graphene oxide hydrogels with enhanced ionic tunability and chemomechanical stability for light-directed 3D printing. Carbon. 2019;143:447-56.
24. Zhang L, Wang Z, Xu C, Li Y, Gao J, Wang W, et al. High strength graphene oxide/polyvinyl alcohol composite hydrogels. Journal of Materials Chemistry. 2011;21(28):10399-406.
25. Bhattacharya S, Samanta SK. Soft-Nanocomposites of Nanoparticles and Nanocarbons with Supramolecular and Polymer Gels and Their Applications. Chemical Reviews. 2016;116(19):11967-2028.
26. Lyon DY, Alvarez PJJ. Fullerene Water Suspension (nC(60)) Exerts Antibacterial Effects via ROS-Independent Protein Oxidation. Environmental Science & Technology. 2008;42(21):8127-32.
27. Belousova IM, Belousov VP, Kiselev VM, Murav'eva TD, Kislyakov IM, Sirotkin AK, et al. Structural and Optical Properties of Solid-Phase Singlet Oxygen Photosensitizers Based on Fullerene Aqueous Suspensions. Optics and Spectroscopy. 2008;105(5):711-9.
28. Mba M, Jiménez AI, Moretto A. Templating the Self-Assembly of Pristine Carbon Nanostructures in Water. Chemistry – A European Journal. 2014;20(14):3888-93.
29. Zhang Y, Zhang H, Zou Q, Xing R, Jiao T, Yan X. An injectable dipeptide-fullerene supramolecular hydrogel for photodynamic antibacterial therapy. Journal of Materials Chemistry B. 2018;6(44):7335-42.
30. Wakai H, Momoi T, Yamauchi T, Tsubokawa N. A Simple Preparation of C60-Poly(ethylene glycol) Gel and its Properties. Polymer Journal. 2009;41(1):40-5.
31. Sugikawa K, Inoue Y, Kozawa K, Ikeda A. Introduction of Fullerenes into Hydrogels via Formation of Fullerene Nanoparticles. ChemNanoMat. 2018;4(7):682-7.
32. Andersen TR, Larsen-Olsen TT, Andreasen B, Böttiger APL, Carlé JE, Helgesen M, et al. Aqueous Processing of Low-Band-Gap Polymer Solar Cells Using Roll-to-Roll Methods. ACS Nano. 2011;5(5):4188-96.
33. Aernouts T, Aleksandrov T, Girotto C, Genoe J, Poortmans J. Polymer based organic solar cells using ink-jet printed active layers. Applied Physics Letters. 2008;92(3):033306.
34. Merland T, Drou C, Legoupy S, Benyahia L, Schmutz M, Nicolai T, et al. Self-Assembly in water of C60 fullerene into isotropic nanoparticles or nanoplatelets mediated by a cationic amphiphilic polymer. Journal of Colloid and Interface Science. 2022;624:537-45.
35. Dutertre F, Benyahia L, Chassenieux C, Nicolai T. Dynamic Mechanical Properties of Networks of Wormlike Micelles Formed by Self-Assembled Comblike Amphiphilic Copolyelectrolytes. Macromolecules. 2016;49(18):7045-53.
36. Limouzin-Morel C, Dutertre F, Moussa W, Gaillard C, Iliopoulos I, Bendejacq D, et al. One and two dimensional self-assembly of comb-like amphiphilic copolyelectrolytes in aqueous solution. Soft Matter. 2013;9(37):8931-7.
37. Milliken J, Keller TM, Baronavski A, McElvany SW, Callahan JH, Nelson H. Thermal and oxidative analyses of buckminsterfullerene, C60. Chemistry of Materials. 1991;3(3):386-7.
38. Deguchi S, Alargova RG, Tsujii K. Stable Dispersions of Fullerenes, C60 and C70, in Water. Preparation and Characterization. Langmuir. 2001;17(19):6013-7.
39. Sinha Ray S, Okamoto M. Polymer/layered silicate nanocomposites: a review from preparation to processing. Progress in Polymer Science. 2003;28(11):1539-641.
40. Hotton C, Sirieix-Plénet J, Ducouret G, Bizien T, Chennevière A, Porcar L, et al. Organisation of clay nanoplatelets in a polyelectrolyte-based hydrogel. Journal of Colloid and Interface Science. 2021;604:358-67.
41. Sprakel J, Spruijt E, Cohen Stuart MA, Besseling NAM, Lettinga MP, van der Gucht J. Shear banding and rheochaos in associative polymer networks. Soft Matter. 2008;4(8):1696-705.
42. Guth E. Theory of Filler Reinforcement. Rubber Chemistry and Technology. 1945;18(3):596-604.
43. Lipatov YS. Polymer reinforcement: ChemTec Publishing; 1995.
44. Shih W-H, Shih WY, Kim S-I, Liu J, Aksay IA. Scaling behavior of the elastic properties of colloidal gels. Physical Review A. 1990;42(8):4772-9.
45. Song Y, Zheng Q. Concepts and conflicts in nanoparticles reinforcement to polymers beyond hydrodynamics. Progress in Materials Science. 2016;84:1-58.
46. Kao P-K, Solomon MJ, Ganesan M. Microstructure and elasticity of dilute gels of colloidal discoids. Soft Matter. 2022;18(7):1350-63.
47. Zhang H, You W, Bian F, Yu W. Heterogeneous Percolation in Poly(methylvinylsiloxane)/Silica Nanocomposites: The Role of

Polymer–Particle Interaction. Macromolecules. 2022;55(19):8834-45.
48. Griffith AA, Taylor GI. VI. The phenomena of rupture and flow in solids. Philosophical Transactions of the Royal Society of London Series A, Containing Papers of a Mathematical or Physical Character. 1921;221(582-593):163-98.